Proceedings of
The Second National Congress on Fluids Engineering
August 22-24, 2002, Muju, Korea

Finite Element Analysis of Electrical Double Layers near Triple Contact Lines

Kwan Hyoung Kang,* In Seok Kang** and Choung Mook Lee***

Key words: *Electrical Double Layer, Contact Angle Saturation, Triple Contact Line, Droplet*

Abstract

To assess the electrostatic interaction of surfaces at the triple contact line, the electrostatic field is analyzed by using the finite element method. The Helmholtz free energy is used as a functional which should be minimized under an equilibrium condition. The numerical results are compared with the nonlinear analytical solution for a two-dimensional charged interface and linear solution for a wedge shaped geometry, which shows fairly good agreement. The method is applied to the analysis of electrostatic influence on the contact angle on a charged substrate. The excess free energy found to increase drastically as the contact angle approaches to zero. This excess free energy plays an opposite role to the primary electrocapillary effect, as the contact angle gets smaller. This enables an alternative explanation for the contact-angle saturation phenomenon occurring in electrical control of surface tension and contact angle.

1. Introduction

The electrical control of wettability of liquid on a solid dielectric substrate, which is called electrowetting or in a broader sense as electrocapillarity, draws renewed attention nowadays in fabricating integrated microfluidic devices such as biochips, microreactors, and μTAS (micro total analysis system) (see [1] for review).

The electrowetting has been mainly understood as a kind of the Lippmann phenomenon which is a direct consequence of electrical polarization of the interface [1-3]. The macroscopic energy balance generates the following modified version of the Young equation in consideration of the electrical effect which predicts the contact angle (θ) for a externally applied electrical potential (V)

$$\cos\theta = \cos\theta_o + \frac{\varepsilon V^2}{2\gamma d}. \tag{1}$$

Here, θ_o is the contact angle without the external electric field, and γ is the interfacial tension between liquid inside the droplet and the surrounding fluid, d the thickness of the dielectric layer beneath the droplet, and ε the electrical permittivity of the dielectric material.

Equation (1) enables an explanation for the near parabolic behavior of the contact angle with respect to the applied electrical potential. There is, however, deficiency in (1) to explain the occurrence of the interfacial instability and saturation of contact angle beyond a certain critical value of electrical potential. Many investigators have suggested their interpretations on the mechanisms to induce such an instability and contact-angle saturation[1,4-6]. None of them is satisfactorily validated to be reliable.

One of the obvious shortcomings of (1), as noted by Digilov[7], is that the effect of the line tension is not considered. The line tension results from the excess free energy generated at the juncture of three interfaces, i.e., liquid-solid, fluid-solid and fluid-liquid. The concept of the line tension is introduced, in a macroscopic analysis concerning the contact angle, to represent the contribution of the excess free energy change due to three-phase interaction near the triple contact line (TPL). Digilov[7] introduced a modified Young equation considering the contribution from the line tension effect, together with the Lippmann phenomena. For a practical assessment of the line-tension effect, the magnitude of the line tension should be known, which cannot be predicted by the macroscopic analysis such as of Digilov[7]. For the analytical prediction on the magnitude of the line tension, the microscopic analysis on the interaction between species near TPL is necessary. In the present investigation, the effect of excess free energy of the charged wedged-shaped geometry on the contact angle is analyzed. It is assumed that the length scale for significant shape change is much greater than the screening length. Under this assumption, the deformation of interface shape due to electrostatic field can be neglected. The free energy is then calculated as a function of the contact angle for straight contact lines.

* Dept. Mech. Eng., Pohang Univ. Sci. & Tech., khkang@postech.edu
** Dept. Chem. Eng., Pohang Univ. Sci. & Tech., iskang@postech.edu
*** Dept. Mech. Eng., Pohang Univ. Sci. & Tech., cmlee@postech.edu

2. Analysis

Two immiscible fluids ionize the substrate differently depending on their chemical properties. The surface-charge density on each region is denoted by σ_1 and σ_2 (see Fig. 1). Here, subscripts 1 and 2 denote, respectively, the fluids inside a droplet and the surrounding fluid, while subscript 3 denotes the quantity associated with the substrate. The surface-charge density at the fluid-fluid interface is denoted by σ_m.

The total free energy of the system (G_{tot}) is the sum of mechanical part (G_{mech}) and electrostatic part (G_{el}) and written as shown below [10-12].

$$G_{mech} = \gamma_{12}\int d\mathbf{S}_{12} + (\gamma_{23}-\gamma_{13})\int d\mathbf{r} + g(\rho_2-\rho_1)\int h^2(\mathbf{r})d\mathbf{r},$$
$$G_{el} = \int\sigma(\mathbf{S})\varphi(\mathbf{S})d\mathbf{S} - \int d\mathbf{r}dy\left[\tfrac{1}{2}\varepsilon(\mathbf{r},y)|\nabla\varphi|^2 + U(\varphi)\right] \tag{2a,b}$$

where γ represents the surface tension, $d\mathbf{r}$ the substrate surface element, $d\mathbf{S}$ the surface element at each interface, $d\mathbf{S}_{12}$ the surface element at fluid-fluid interface, $U(\varphi) = 2n^{\infty}kT[\cosh(\beta\varphi)-1]$, φ the electrical potential, $\beta \equiv ze/kT$, ε the electric permittivity, k the Boltzmann constant, T the absolute temperature, z the valence of ions, e the electron charge, and n^{∞} the number density

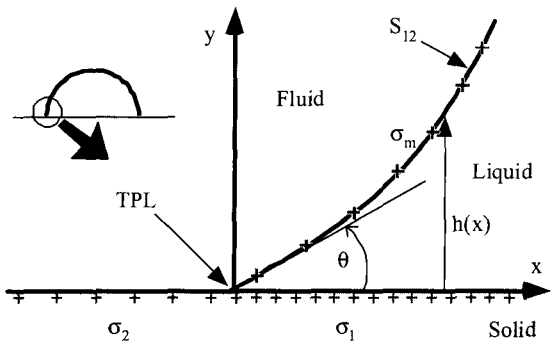

Fig. 1 Geometry of a droplet on a charged substrate in the proximity of contact line. Interface is charged due to adsorption of charged species.

of ion at the bulk region. The terms in (2) are the surface energy associated with the area of the droplet surface exposed to the bulk fluid, the energy of contact of the two fluids with solid substrate, the gravitational energy arising from the density difference between interior and exterior fluids, and the electrostatic contributions for specified surface charge distribution [10].

Far from the TPL, the electrical contribution to the free energy per unit surface area becomes

$$g_{el} = 2\frac{\varepsilon\kappa}{\beta^2}\left[2 - 2\cosh\frac{\beta\varphi_s}{2} + \beta\varphi_s \sinh\frac{\beta\varphi_s}{2}\right], \tag{3}$$

where φ_s represent the electrical potential at interfaces, and $\kappa_j^2 = e/\varepsilon_j \cdot \sum_i z_i^2 n_i^{\infty}$ the inverse square of the Debye screening length. In the present investigation, only the electrostatic contribution to the excess free energy is considered. Other contributions to the line tension, such as due to the short range forces[13], are beyond the scope of the present investigation. The total free energy of the system can be alternatively expressed by employing the contribution due to the line-tension (τ), as follows

$$\begin{aligned} G_{tot} &= G_{mech} + G_{el} \\ &= G_{mech} + G_{el,b} + \tau L = G_{mech} + \oint g_{el}\, d\mathbf{S} + \tau L. \end{aligned} \tag{4}$$

Here, L is the length of TPL, and becomes $2\pi R$ for an axially symmetric droplet having base radius of R. $G_{el,b}$ represents the electrical free energy of the system calculated by the unperturbed electrostatic potential at far distance from the TPL. This term is dependent on the interfacial areas, but not on the specific geometry of a droplet.

We non-dimensionalize the variables by using the screening length, and characteristic thermal energy ($1/\beta = kT/ze$) as

$$\tilde{x} = \kappa_2 x,\ \tilde{y} = \kappa_2 y,\ \tilde{\varphi}_j = \beta\varphi_j, \tilde{\sigma}_j = \frac{\beta\sigma_j}{\varepsilon_2\kappa_2},\ \tilde{G}_{el} = \frac{\kappa_2\beta^2}{\varepsilon_2} G_{el}. \tag{5}$$

Then, the electrostatic free-energy components can be rewritten as shown below. The tilde is dropped for the sake of convenience.

$$G_{el} = \int \sigma(\mathbf{S})\varphi(\mathbf{S}) d\mathbf{S} - \int d\mathbf{r}dy \left[\tfrac{1}{2}\bar{\varepsilon}(\mathbf{r}, y)|\nabla\varphi|^2 + \bar{\varepsilon}\bar{\kappa}^2 U[\varphi]\right], \tag{6a}$$

$$G_{el,b} = \oint 2\bar{\varepsilon}\bar{\kappa}\left[2 - 2\cosh\frac{\varphi_s}{2} + \varphi_s \sinh\frac{\varphi_s}{2}\right] d\mathbf{S}. \tag{6b}$$

Here, $\bar{\varepsilon} = \varepsilon/\varepsilon_2$, $\bar{\kappa} = \kappa/\kappa_2$, and $U[\varphi] = \cosh\varphi - 1$.

The mechanical part of the free energy is not directly concerned with the electrical potential. Therefore, during the solution procedure for electrical potential, only the electrical part is considered. The potential distribution is analyzed by using the finite element method. It is natural to choose the above free energy as the functional to be minimized. For each discretized element, the potential function $\varphi^{(e)}$ can be represented as a linear combination of shape function $N(x, y)$, i.e.,

$$\varphi^{(e)} = \sum_{i=1}^{m} \varphi_i N_i(x, y) \tag{7}$$

where m is the number of nodes in an element and φ_i are the discrete nodal potentials. In the present investigation, the six-node triangular elements with the Lagrange polynomial are used. (For details, on the finite element formulation, see Appendix I).

3. Results and Discussion

Figure 2 shows the electrical potential for a charged infinite planar interface case. In the figure, ξ denotes the normal distance from the interface. This one-dimensional solution is obtained by applying appropriate boundary conditions for the identical program used in the two-dimensional analysis. Here, $\bar{\kappa}_1 = 1$, and $\bar{\varepsilon}_1 = 0.2$. The two cases in which σ_m is 8 and 32 are shown in the figure. The results are compared with the linear and nonlinear solution of the Poisson-Boltzmann equation (see Appendix II). The numerical solutions show a good agreement with the fully nonlinear analytical solutions. The linear solution, however, tends to overestimate the peak potential values for $\sigma_m = 32$. These are mainly because the linearization of the source term in the Poisson-Boltzmann has an effect to reduce the charge density of field ions. For example, the linearization of charge density, i.e., approximating $\sinh\varphi$ as φ, when $\varphi = 1$, has an effect to reduce the charge density by 17.5% with respect to the exact value. For high potential values, the error becomes greater.

Figure 3 shows the electrical potential at the TPL for different contact angles. In this case too, the screening lengths are assumed to be the same for the two fluids, and $\bar{\varepsilon}_1 = 4$. The linear analysis of the Poisson-Boltzmann equation for the electrical potential near the TPL[10]

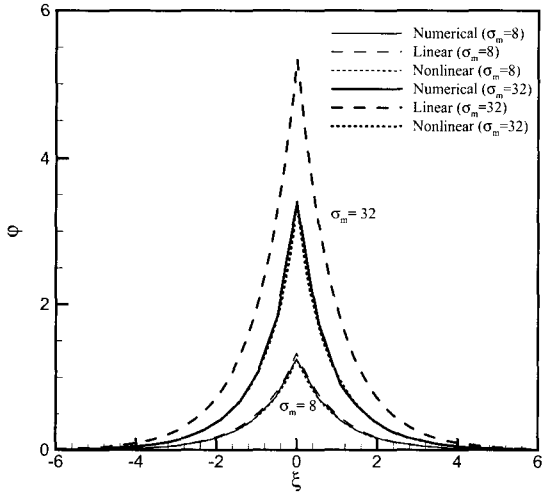

Fig. 2 Validation of numerical results for a charged planar interface: $\kappa_1 = \kappa_2$, $\bar{\varepsilon} = 0.2$

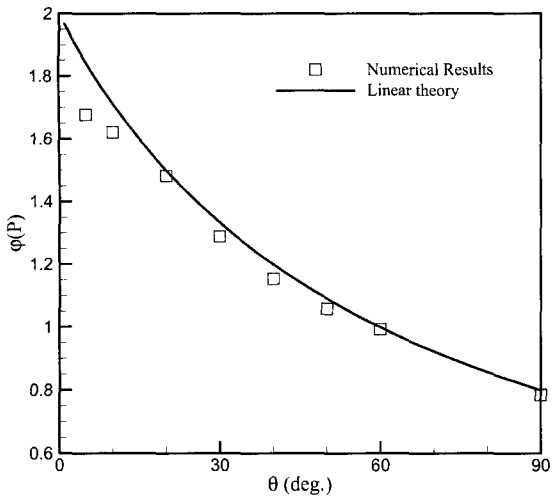

Fig. 3 Potential at contact line for different contact angle: $\sigma_1 = \sigma_2 = 1$, $\sigma_m = 2$, $\kappa_1 = \kappa_2$, $\bar{\varepsilon} = 4$.

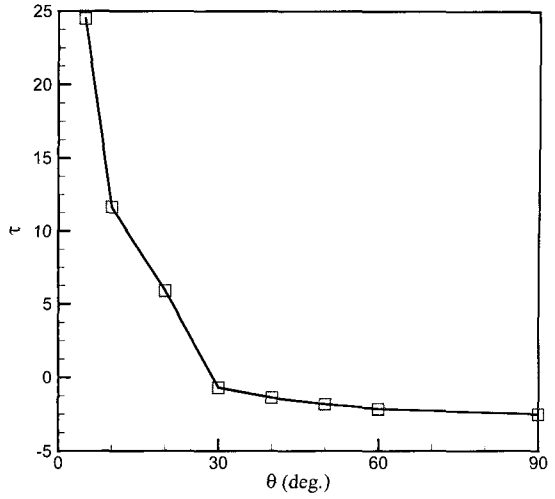

Fig. 4 Electrostatic contribution to the line tension for different contact angle: $\sigma_1 = \sigma_2 = 1$, $\sigma_m = 2$, $\kappa_1 = \kappa_2$, $\bar{\varepsilon} = 4$.

gives the following potential at TPL, when $\kappa_1 = \kappa_2$,

$$\varphi(P;\theta) \cong \left(\frac{1}{2}\right) \cdot \frac{\sigma_1 + \sigma_2 + \sigma_m}{[(\bar{\varepsilon} - 1) \cdot \theta / \pi + 1]} \cdot \tag{8}$$

As shown in the figure, the present results agree very well with the linear solution when the contact angle is greater than 30°. At a smaller contact angle than about 30°, the deviation becomes greater as the contact angle gets smaller. This may be because, alike the case in Fig. 2, the effect of field charge is underestimated due to the linearization.

Figure 4 shows the line tension which is related with the excess free energy as (4) for different contact angles, for the same conditions considered in Fig. 3. As the contact angle decreases, the excess free energy increases abruptly. This means there is a tendency to resist against the contact of the two interfaces.

If the free energy minimum principle under the thermodynamic equilibrium condition is applied to (4) through the method of variational calculus, the following formula for the equilibrium contact angle is obtained,

$$\cos\theta = \cos\theta_o + PECE - \frac{\tau(\theta)}{\gamma R} \cdot \tag{9}$$

Here, *PECE* represents the contribution due to the primary electrocapillary effect which becomes $\frac{1}{2}\varepsilon V^2/(\gamma d)$ for the electrowetting case. As shown in Fig. 4, the line tension has positive values and gets greater as the radius of droplet approaches to zero. Therefore, its influence becomes amplified when the size of a droplet becomes smaller, which is customary among the line-tension effect. Moreover, in the case of small contact angle, the line tension due to surface charge has in general opposite role compared to the primary electrocapillary effect. This can results in the saturation of contact angle under a high electric field, when the contact angle is controlled by electrical means.

4. Concluding Remarks

The computed results by using the finite element method show a good agreement with the analytical solutions. The excess free energy becomes very large when the contact angle becomes small. When the contact angle is small, excess free energy has opposite sign to the term representing the conventional electrocapillary effect. Therefore, the usual electrocapillary effect of decreasing the contact angle can be reduced. Furthermore, the contact angle can be saturated due to significantly amplified line-tension effect for small contact angle. The line-tension effect becomes more influential for droplets of smaller size.

In the present investigation, the effect of deformation of interface is not considered. The interface will be deformed when the pressure near the interface becomes greater. In this case, the electric field can be significantly distorted due to interfacial deformation. The consideration of shape deformation is necessary in the future analysis.

Acknowledgement

The present investigation was carried out as a part of the project of Brain Korea 21 and an internal basic research program of Pohang University of Science and Technology (POSTECH). The authors gratefully acknowledge the funding support for the present investigation by Korean Ministry of Education and Human Resource Development and POSTECH.

Appendix I. Formulation for finite element analysis

Substituting the approximated potential into the free energy functional, one can obtain the discretized functional for an element such as

$$G_{el}^{(e)}(\varphi^{(e)}) = \sum_{i=1}^{r} \varphi_i \int_{\Gamma^{(e)}} \sigma N_i d\Gamma^{(e)} - \frac{1}{2}\sum_{i=1}^{r}\sum_{j=1}^{r} \varphi_i \varphi_j \int_{\Omega^{(e)}} \bar{\varepsilon} \nabla N_i \cdot \nabla N_j d\Omega^{(e)} - \sum_{i=1}^{r} \int_{\Omega^{(e)}} \bar{\varepsilon}\bar{\kappa}^2 U_i(\varphi) N_i d\Omega^{(e)} \tag{A1}$$

This can be rewritten in a matrix form as

$$G_{el}^{(e)}(\varphi^{(e)}) = \{\varphi\}^T \{R\} - \frac{1}{2}\{\varphi\}^T [S]\{\varphi\} - \{U(\varphi)\}^T \{Q\} \tag{A2}$$

where

$$R_i = \int_{\Gamma^{(e)}} \sigma N_i d\Gamma^{(e)},$$
$$S_{ij} = \int_{\Omega^{(e)}} \bar{\varepsilon} \nabla N_i \cdot \nabla N_j d\Omega^{(e)}, \quad \text{(A3a,b,c)}$$
$$Q_i = \int_{\Omega^{(e)}} \bar{\varepsilon} \bar{\kappa}^2 N_i d\Omega^{(e)} \cdot$$

The total electrical contribution to the free energy of the domain is the sum of the free energy of the individual element, that is $G_{el} = \sum_e G_{el}^{(e)}$. This can be represented in a matrix form as

$$G_{el} = \sum_e \left[\{\varphi\}^T \{R\} - \tfrac{1}{2} \{\varphi\}^T [S] \{\varphi\} - \{U(\varphi)\}^T \{Q\} \right]. \quad \text{(A4)}$$

At an equilibrium condition, G_{el} should be minimized with respect to electrostatic potential, that is, $\partial G_{el}^{(e)} / \partial \varphi_i = 0$, for $i = 1,2,...,m$. This requirement results in the following matrix equation

$$[S]\{\varphi\} = \{R\} - \{Q'\}, \quad \text{(A5)}$$

where

$$Q_i' = \int_{\Omega^{(e)}} \bar{\kappa}^2 U_i'(\varphi) N_i d\Omega^{(e)} = \int_{\Omega^{(e)}} \bar{\varepsilon} \bar{\kappa}^2 \sinh(\varphi_i) N_i d\Omega^{(e)} \cdot \quad \text{(A6)}$$

Appendix II. Electrical double layer at a charged fluid interface

Far from the triple contact line in Fig. 1, the following Poisson-Boltzmann equation which accounts for the Coulombic interaction between electrical charge is satisfied.

$$\frac{\partial^2 \varphi_j}{\partial \xi^2} = \kappa_j^2 \left(\frac{kT}{ze} \right) \sinh \frac{ze\varphi_j}{kT}, \text{ for each fluid } j = 1, 2. \quad \text{(B1)}$$

The boundary conditions which should be satisfied by the electrical potentials are as follows:

$$\text{i)} \ \varphi_1 = \varphi_2, \text{ at } \xi = 0, \quad \text{(B2a)}$$
$$\text{ii)} \ \varepsilon_2 \frac{\partial \varphi_2}{\partial \xi} - \varepsilon_1 \frac{\partial \varphi_1}{\partial \xi} = \sigma_m, \text{ at } \xi = 0, \quad \text{(B2b)}$$
$$\text{iii)} \ \varphi_j = 0, \text{ at } \xi = \pm\infty. \quad \text{(B2c)}$$

The following relation holds for each region,

$$\frac{\partial}{\partial x} \left(\frac{\partial \varphi}{\partial \xi} \right)^2 = 2 \frac{\partial \varphi}{\partial \xi} \frac{\partial^2 \varphi}{\partial \xi^2}, \quad \frac{\partial^2 \varphi}{\partial \xi^2} = \frac{1}{2} \frac{\partial}{\partial \varphi} \left(\frac{\partial \varphi}{\partial \xi} \right)^2. \quad \text{(B3a,b)}$$

Introducing (B1) to (B3b), integrating both side with respect to φ, applying the boundary condition in (B2c), and then one obtains.

$$\left(\frac{\partial \varphi_j}{\partial \xi} \right)^2 = 2 \frac{\kappa^2}{\beta^2} (\cosh \beta \varphi_j - 1) \cdot \quad \text{(B4)}$$

By using the relation that $\cosh 2x - 1 = 2 \sinh^2 x$, the above equation also becomes

$$\frac{\partial \varphi_1}{\partial \xi} = -2 \frac{\kappa_1}{\beta} \sinh \frac{\beta \varphi_1}{2}, \quad \frac{\partial \varphi_2}{\partial \xi} = 2 \frac{\kappa_2}{\beta} \sinh \frac{\beta \varphi_2}{2} \cdot \quad \text{(B5a,b)}$$

Applying (B5) to the interfacial boundary condition (B2b) with (B2a), then one obtains the following nonlinear algebraic equation for the interface potential φ_I,

$$\frac{2}{\beta} (\varepsilon_1 \kappa_1 + \varepsilon_2 \kappa_2) \sinh \frac{\beta \varphi_I}{2} = \sigma_m \cdot \quad \text{(B6)}$$

Integration of (A6a,b) yields the following potential distribution for each region.

$$e^{\beta \varphi_j / 2} = \frac{e^{\beta \varphi_I / 2} + 1 + (e^{\beta \varphi_I / 2} - 1) e^{-\kappa_j |\xi|}}{e^{\beta \varphi_I / 2} + 1 - (e^{\beta \varphi_I / 2} - 1) e^{-\kappa_j |\xi|}}. \quad \text{(B7)}$$

The solution of the linearized Poisson-Boltzmann equation for this case can be obtained as follows, without difficulty.

$$\varphi_j = \varphi_I e^{-\kappa_j |\xi|}, \quad \text{(B8a)}$$
$$(\varepsilon_1 \kappa_1 + \varepsilon_2 \kappa_2) \varphi_I = \sigma_m \cdot \quad \text{(B8b)}$$

References

[1] C. Quilliet and B. Berge (2001) "Electrowetting: a recent outbreak," *Current Opinion in Colloid and Interface Science* 6, 34-39.

[2] T. D. Blake, A. Clarke, and E. H. Stattersfield (2000) "An investigation of electrostatic assist in dynamic wetting," *Langmuir* 16, 2928-2935.

[3] M. W. J. Prins, W. J. J. Welters, and J. W. Weekamp (2001) "Fluid Control in Multichannel Structures by Electrocapillary Pressure," *Science*, January 12.

[4] M. Vallet, M. Vallade, and B. Berge (1999) "Limiting phenomena for the spreading of water on polymer films by electrowetting," *Eur. Phys. J. B.* 11, 583-591.

[5] H. J. J. Verheijen, M. W. J. Prins (1999) "Reversible electrowetting and trapping of charge: Model and experiments," *Langmuir*, 15 (20), 6616-6620.

[6] V. Peykov, A. Quinn, J. Ralston (2000) "Electrowetting: a model for contact-angle saturation," *Colloid & Polymer Science*, 278 (8), 789-793.

[7] R. Digilov (2000) "Charge-induced modification of contact angle: the secondary electrocapillary effect," *Langmuir* 16, 6719-6723.

[8] B. Duplantier (1991) "Can one "hear" the thermodynamics of a (rough) colloid?" *Phys. Rev. Lett.* 66(12), 1555.

[9] Y. Solomentsev, and L. R. White (1999) "Microscopic drop profiles and the origins of line tension," *J. Colloid Interface Sci.* 218, 122-136.

[10] T. Chou (2001) "Geometry-dependent electrostatics near contact lines," *Physical Review Letters* 87 (10), 106101.

[11] T. Chou, M .V. Jarić, and E. D. Siggia (1997) "Electrostatics of lipid bilayer bending," *Biophysical Journal* 72, 2042-2055.

[12] Y. Burak and D. Andelman (2000) "Hydration interactions: Aqueous solvent effects in electric double layers," *Physical Review E* 62(4), 5296-5312.

[13] P. G. de Gennes (1985) "Wetting: statics and dynamics," Review of Modern Physics 57(3), 827-863.

[14] B. Janocha, H. Bauser, C. Oehr, H. Brunner, and W. Göpel (2000) "Competitive electrowetting of polymer surfaces by water and decane," *Langmuir*, *16*, 3349-3354.